UCLA
UCLA Previously Published Works

Title

Rapid degradation of mutant SLC25A46 by the ubiquitin-proteasome system results in MFN1/2-mediated hyperfusion of mitochondria.

Permalink

https://escholarship.org/uc/item/8kw5z8s7

Journal

Molecular biology of the cell, 28(5)

ISSN

1059-1524

Authors

Steffen, Janos
Vashisht, Ajay A
Wan, Jijun
et al.

Publication Date

2017-03-01

DOI

10.1091/mbc.e16-07-0545

Peer reviewed

eScholarship.org Powered by the California Digital Library
University of California

Rapid degradation of mutant SLC25A46 by the ubiquitin-proteasome system results in MFN1/2-mediated hyperfusion of mitochondria

Janos Steffen[a], Ajay A. Vashisht[b], Jijun Wan[c], Joanna C. Jen[c], Steven M. Claypool[d], James A. Wohlschlegel[b,e], and Carla M. Koehler[a,e,f,*]

[a]Department of Chemistry and Biochemistry, [b]Department of Biological Chemistry, David Geffen School of Medicine, [c]Department of Neurology, [e]Molecular Biology Institute, and [f]Jonsson Comprehensive Cancer Center, University of California, Los Angeles, Los Angeles, CA 90095, [d]Department of Physiology, Johns Hopkins University School of Medicine, Baltimore, MD 21205

ABSTRACT **SCL25A46 is a mitochondrial carrier protein that surprisingly localizes to the outer membrane and is distantly related to Ugo1. Here we show that a subset of SLC25A46 interacts with mitochondrial dynamics components and the MICOS complex. Decreased expression of SLC25A46 results in increased stability and oligomerization of MFN1 and MFN2 on mitochondria, promoting mitochondrial hyperfusion. A mutation at L341P causes rapid degradation of SLC25A46, which manifests as a rare disease, pontocerebellar hypoplasia. The E3 ubiquitin ligases MULAN and MARCH5 coordinate ubiquitylation of SLC25A46 L341P, leading to degradation by organized activities of P97 and the proteasome. Whereas outer mitochondrial membrane–associated degradation is typically associated with apoptosis or a specialized type of autophagy termed mitophagy, SLC25A46 degradation operates independently of activation of outer membrane stress pathways. Thus SLC25A46 is a new component in mitochondrial dynamics that serves as a regulator for MFN1/2 oligomerization. Moreover, SLC25A46 is selectively degraded from the outer membrane independently of mitophagy and apoptosis, providing a framework for mechanistic studies in the proteolysis of outer membrane proteins.**

Monitoring Editor
Thomas D. Fox
Cornell University

Received: Jul 26, 2016
Revised: Dec 12, 2016
Accepted: Dec 30, 2016

INTRODUCTION

The mitochondrial network is maintained by a combination of fusion and fission events. Defects in this fine balance can cause numerous diseases, including cancer, cardiac disease, and particularly neurodegeneration (Archer, 2013). Fission and fusion are regulated by a small subset of dynamin-related guanosine triphosphatases (GTPases) located in the cytosol or inner (IM) and outer (OM) mitochondrial membranes. On activation, the dynamin-related protein 1 (DRP1) oligomerizes on mitochondria, forming a ring-like structure that constricts and finally divides the mitochondria. Fusion is mediated by the GTPases optic atrophy 1 (OPA1) on the IM and mitofusins 1 and 2 (MFN1 and MFN2) on the OM. OPA1 consists of approximately eight mRNA OPA1 isoforms in humans (Delettre *et al.*, 2001). IM-bound long (L)-OPA1 forms can be processed by proteolytic cleavage to generate short (S)-OPA1 (Ishihara *et al.*, 2006). OM fusion is regulated by MFN1 and MFN2 (Santel and Fuller, 2001; Chen *et al.*, 2003). MFN1 and MFN2 form homo- and hetero-oligomers on the OM and are required for an elongated mitochondrial network (Detmer and Chan, 2007). Deletion of MFN1 or MFN2 is embryonic lethal. Moreover, MFN1 and MFN2 differ in their expression in various tissues (Bertholet *et al.*, 2016), which may result in independent functions. Whereas mutations in MFN2 are associated with ~20% of Charcot–Marie–Tooth (CMT) type 2 cases—an inherited peripheral neuropathy (Züchner *et al.*, 2004; Verhoeven *et al.*, 2006)—no disease has been associated with mutations in MFN1.

Misfolded proteins within mitochondria are removed by the coordinated action of chaperones and proteases (Quiros *et al.*, 2015).

This article was published online ahead of print in MBoC in Press (http://www.molbiolcell.org/cgi/doi/10.1091/mbc.E16-07-0545) on January 5, 2017.

The authors declare no competing financial interests.

*Address correspondence to: Carla Koehler (koehler@chem.ucla.edu).

Abbreviations used: BN, blue-native; CFTR, cystic fibrosis transmembrane conductance regulator; CMT, Charcot–Marie–Tooth; coIP, coimmunoprecipitation; CRL, Cullin RING ligase; DMSO, dimethyl sulfoxide; HA, hemagglutinin; IM, inner mitochondrial membrane; OM, outer mitochondrial membrane; PCH, pontocerebellar hypoplasia; shRNA, short hairpin RNA; UPS, ubiquitin-proteasome system.

© 2017 Steffen *et al.* This article is distributed by The American Society for Cell Biology under license from the author(s). Two months after publication it is available to the public under an Attribution–Noncommercial–Share Alike 3.0 Unported Creative Commons License(http://creativecommons.org/licenses/by-nc-sa/3.0).

"ASCB®," "The American Society for Cell Biology®," and "Molecular Biology of the Cell®" are registered trademarks of The American Society for Cell Biology.

The ubiquitin-proteasome system (UPS) removes proteins from the OM (Campello *et al.*, 2014). Typical substrates are proteins involved in mitochondrial dynamics and apoptosis (Karbowski and Youle, 2011). Several E3 ubiquitin ligases have been associated with mitochondria. The RING E3 ligase MARCH5/MITOL is a multispanning OM protein that ubiquitylates primary substrates DRP1 and FIS1 (Nakamura *et al.*, 2006; Yonashiro *et al.*, 2006; Karbowski *et al.*, 2007). MULAN/MAPL/MUL1 is another RING E3 ligase anchored to the mitochondrial OM that ubiquitylates MFN1/2 and sumoylates DRP1 (Braschi *et al.*, 2009; Lokireddy *et al.*, 2012). A few cytosolic E3 ligases, such as PARKIN and HUWE1/MULE/HECTH9, are recruited to mitochondria and ubiquitylate MFN2 and other OM substrates to activate mitophagy and apoptosis, respectively (Narendra *et al.*, 2008; Leboucher *et al.*, 2012). The E3 ligases likely have overlapping specificities to maintain OM homeostasis and regulate mitophagy. For example, MULAN acts in parallel to the PINK1-PARKIN pathway, and different E3 ligases seem to have differing importance in different tissues and conditions (Livnat-Levanon and Glickman, 2011; Yun *et al.*, 2014). After ubiquitylation, OM proteins are extracted from the membrane by the AAA ATPase P97/VCP and subsequently degraded by the proteasome in the cytosol (Heo *et al.*, 2010; Tanaka *et al.*, 2010).

In a recent study (Wan *et al.*, 2016), we found that SLC25A46 is an OM protein that, when deleted or mutated (L341P), leads to hyperfused mitochondria and finally to lethal pontocerebellar hypoplasia (PCH). Similar results focused on different mutations in SLC25A46 have been recently published (Abrams *et al.*, 2015; Janer *et al.*, 2016). Mutations in SLC25A46 have been associated with dominant optic atrophy (DOA) and CMT type 2, and the mitochondria have increased mitochondrial connectivity (Abrams *et al.*, 2015). In addition, a family with a missense mutation in SLC25A46 exhibited Leigh syndrome, and the physiological phenotype was characterized by defects in mitochondrial lipid homeostasis, cristae maintenance, and bioenergetics (Janer *et al.*, 2016).

In this study with cell models, the underlying cause of PCH is likely loss of function from selective degradation of SLC25A46 that harbors a mutation in the putative fifth membrane-spanning domain. Here we study the underlying mechanism resulting in hyperfusion of mitochondria and the specific pathway for selective degradation of mutant SLC25A46 L341P. We show that MFN1 and MFN2 accumulate on mitochondria in an oligomeric state in cells lacking SLC25A46 or expressing SLC25A46 L341P, which results in enhanced fusion. Further, our data indicate that MARCH5 and MULAN coordinate the degradation of SLC25A46 and seem to have redundant functions.

RESULTS

SLC25A46 associates with several OM proteins, particularly components in mitochondrial dynamics

In a previous study, we found that rare cases of PCH were likely caused by a deletion in exon 1 (causing gene disruption) or a point mutation in exon 8 in mitochondrial OM protein SLC25A46 (leucine at position 341 is replaced with proline, designated L341P (Wan *et al.*, 2016); SLC25A46 L341P was not stable, and the mitochondria displayed hyperfused mitochondria and other aberrant morphologies (Wan *et al.*, 2016). To investigate the potential function of SLC25A46, we performed immunoprecipitations and mass spectrometry analysis on mitochondria isolated from a stable HEK293T cell line expressing wild-type (WT) SLC25A46 tagged with a 2× hemagglutinin (HA) epitope at the N-terminus. A tag placed at either the N- or the C-terminus did not interfere with insertion into the mitochondrial OM (Supplemental Figure S1A; Abrams *et al.*, 2015; Janer *et al.*, 2016; Wan *et al.*, 2016). After lysis in 1% digitonin, SLC25A46 mostly interacted with proteins involved in fission and fusion such as MFN1/2 or OPA1 and with components of the MICOS complex (Supplemental Table S1). A subset of these potential interaction partners was confirmed by a variety of approaches. First, we solubilized mitochondria that contained SLC25A46 with an N-terminal HA tag in 1% digitonin and used glycerol gradients to examine the distribution of mitochondrial proteins (Figure 1A). SLC25A46 WT mostly migrated near the center of the gradient in fractions 7–13. Migration of OM proteins MFN1 and MTCH2 was also enriched in similar fractions as the SLC25A46 WT protein. Instead, MIC60, MIC27, and MIC19 of the MICOS complex and TOMM40 migrated in heavier fractions (Bohnert *et al.*, 2015; Friedman *et al.*, 2015). Additional controls included PNPase and YME1L of the intermembrane space, TIMM23 in the IM, and matrix-localized PreP and LRP130, which all showed a different distribution pattern than SLC25A46. To assess SLC25A46 and MFN1 binding, analysis of coimmunoprecipitation (coIP) fractions 9, 11, and 13 revealed that a subset of MFN1 and MFN2 indeed interacted with SLC25A46 (Figure 1B). The interactions between SLC25A46 and MFN1/MFN2 were specific because OM protein MID51 did not copurify with SLC25A46 WT or L341P in similar coIP experiments (Figure 2A). We also used the glycerol gradient system to probe the assembly of SLC25A46 L341P from a similar cell line—a stable HEK293T cell line expressing 2xHA-SLC25A46 L341P. In contrast, SLC25A46 L341P was less abundant and sedimented in fractions 17–23, near the bottom of the gradient (Figure 1A and Supplemental Figure S1B). Complexes of TOMM40, MFN1 and MIC60 were not altered in mitochondria with SLC25A46 L341P (Supplemental Figure S1B).

Using blue-native (BN) gels, we also investigated the migration of SLC25A46 WT and L341P, as well as that of partner proteins. The majority of SCL25A46 WT was at a molecular mass of 70–200 kDa, but larger complexes were also identified (Figure 1C). In contrast, the majority of SCL25A46 L341P migrated at a larger size, >600 kDa, but SLC25A46 L341P could be detected throughout the gel. In mitochondria from LAN5 neuronal cells (Figure 1D), endogenous SLC25A46 migrated in similar-sized complexes as in HEK293T cells expressing HA-SCL25A46. MFN1, MFN2, and MTCH2 also comigrated with SLC25A46 (Figure 1, C–E; MFN1/2–SLC25A46 complex [■] and MTCH2–SLC25A46 complex [▲]), and a small amount of SLC25A46 was detected in the larger complex that comigrated with MIC19 and MIC60 (Figure 1, D and E; MICOS–SLC25A46 complex is marked with an asterisk). TOMM40 did not comigrate with SLC25A46 (Figure 1C). Complexes of TOMM40, MFN1, and MIC60 were not altered in mitochondria with SLC25A46 L341P (Supplemental Figure S1B). Thus the BN-gel assay supports that mutation L341P in SLC25A46 alters its complex formation. Moreover, the WT SLC25A46 comigrated with dynamics proteins MFN1 and MFN2 in addition to MTCH2, and a small amount of SLC25A46 comigrated with the MICOS complex. In sum, SLC25A46 associates with several proteins and may function as a scaffold for assembly of proteins involved in mitochondrial ultrastructure.

Because the interactions between SLC25A46 and protein partners may be transient or weak, we performed intracellular cross-linking followed by cell solubilization and coIP assays (Figure 2A). This seemed to trap interactions because SLC25A46 coprecipitated with OPA1 (short and long forms; DeVay *et al.*, 2009), MFN1, MFN2, and MICOS components MIC60 and MIC19. This agrees with our previous study (Wan *et al.*, 2016) and recent publications that SLC25A46 is a component similar to yeast Ugo1, which maintains mitochondrial morphology (Abrams *et al.*, 2015; Janer *et al.*, 2016). In addition, TOMM40 interacted with SLC25A46, which

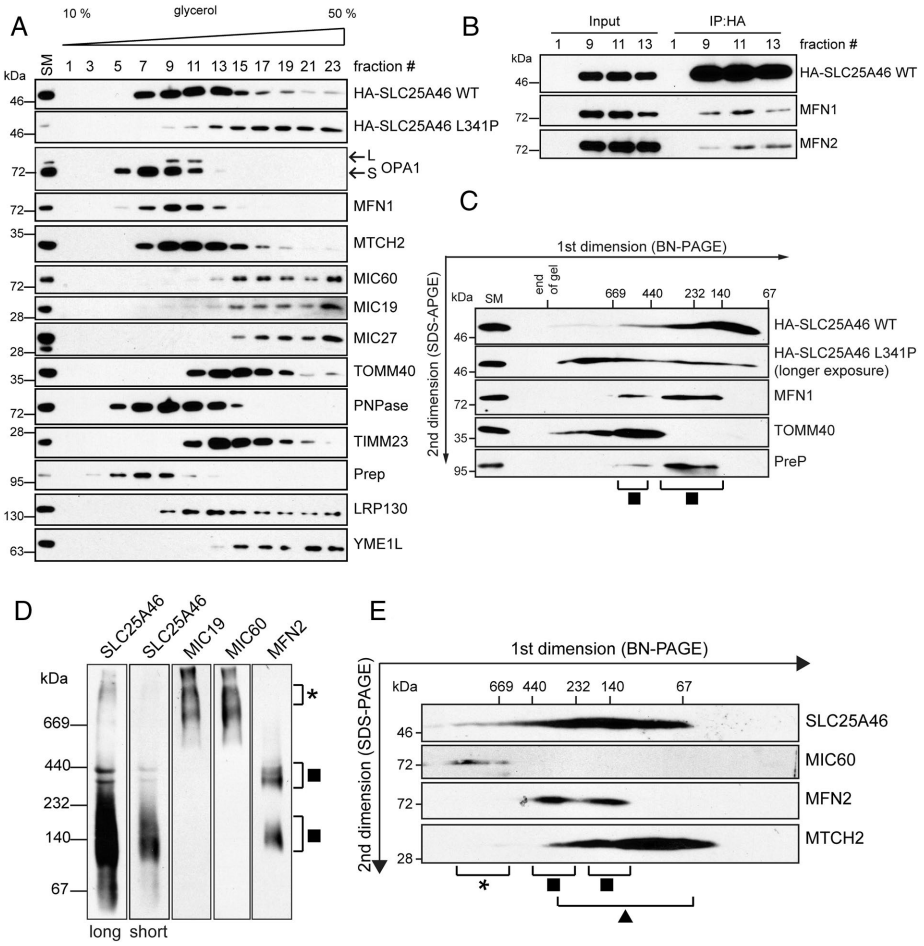

FIGURE 1: SLC25A46 comigrates with mitochondrial dynamics and MICOS proteins. (A) Glycerol gradient density centrifugation of mitochondrial extracts generated from a stable cell line expressing 2xHA-SLC25A46 WT. Mitochondria were solubilized in 1% digitonin, and lysates were loaded on a linear 10–50% glycerol gradient and centrifuged overnight. Fractions 1–23 were analyzed with the indicated antibodies. A similar sample was included, and the HA antibody was used to determine SLC25A46 L341P assembly. SM, starting material. (B) Immunoprecipitation (IP) with the HA antibody of 2xHA-SLC25A46 WT from the indicated fractions (1, 9, 11,13) of the glycerol gradient density centrifugation in A. Input samples correspond to 10% of each fraction. Antibodies against HA, MFN1, and MFN2 were used. (C) Mitochondria isolated form HEK293T cells stably expressing 2xHA-SLC25A46 WT or L341P were solubilized with digitonin, and mitochondrial extracts were resolved by two-dimensional BN-PAGE. Antibodies against MFN1, TOMM40, PreP, and HA were used for immunoblotting. For MFN1, TOMM40, and PreP, the analysis from WT mitochondria is shown, and the complexes migrated identically in mitochondria from the SLC25A46 L341P cell line. (■) The MFN1-SLC25A46 complex. (D, E) Mitochondria were isolated from LAN5 cells and then lysed in 1% digitonin. Mitochondrial extracts were resolved by one- (D) or two- (E) dimensional BN-PAGE; antibodies for endogenous SLC25A46, MIC19, MIC60, MFN2, and MTCH2 were included. In D, shorter and longer exposures for SLC25A46 are shown to highlight the larger complex that comigrates with the MICOS complex. (■) The MFN1-SLC25A46 complex; (▲) the MICOS-SLC25A46 complex; (*) the MTCH2-SLC25A46 complex.

may reflect a role for TOMM40 in SLC25A46 assembly. SCL25A46 L341P also bound to similar proteins but showed an increased binding with TOMM40, MTCH2, and MULAN, an E3 ubiquitin ligase that functions in turnover of OM proteins (Braschi *et al.*, 2009; Ambivero *et al.*, 2014; Yun *et al.*, 2014). However, SLC25A46 did not display strong binding to MIC27. To confirm specificity of SLC25A46 interactions with OM proteins, we found that MID51 did not copurify with SLC25A46 (Figure 2A). This immunoprecipitation experiment under cross-linking conditions supports that SLC25A46 interactions with partner proteins may be transient and require a method such as cross-linking for stabilization.

The clustered regularly interspaced short palindromic repeats (CRISPR)/Cas9 system was used to knock out *SLC25A46* from the HCT116 cell line. *SLC25A46* was successfully deleted, and three representative monoclonal cell lines (designated 1.7, 4.1, 4.3 *SLC25A46* $^{-/-}$) were chosen for additional characterization. The analysis of steady-state levels of partner proteins identified in Figure 2A was tested by immunoblotting (Figure 2B). The abundance of most of these proteins was not altered, indicating that SLC25A46 is not a bona fide partner protein with the MICOS complex. However, we observed a slight increase in the levels of mitochondrial dynamics proteins MFN1 and MFN2 (Figure 2B). We also observed increased steady-state levels of MFN1 and MFN2 in mitochondria when *SLC25A46* was knocked out in the cell line HEK293 T-REx Flp-In (Figure 2, C and D). Specifically, the abundance of MFN1/2 increased ~1.6- and 2-fold, respectively (Figure 2D). To analyze whether these elevated levels were caused by enhanced protein import, we imported radiolabeled MFN1-13myc and MFN2-20myc (Chen *et al.*, 2003) into isolated mitochondria from WT and *SLC25A46*$^{-/-}$ HEK293 T-REx Flp-In cells and analyzed the import by SDS–PAGE and BN-PAGE (Supplemental Figure S2, A and B). The presence of the additional myc tags on the C-terminus of MFN1 and MFN2 does not interfere with function or assembly (Chen *et al.*, 2003) but results in increased molecular weight (Supplemental Figure S2, A and B). Imported MFN1 and MFN2 were recovered in the pellet fraction after alkali extraction. For both proteins, we did not observe any changes in protein import. We also included control import reactions that lacked mitochondria to confirm that MFN1 and MFN2 did not nonspecifically fraction in the pellet after alkali extraction; MFN1 and MFN2 were not recovered in the pellet fraction in the absence of mitochondria (Supplemental Figure S2A). We also did not note any differences in *MFN1* and *MFN2* expression in HEK293 T-REx Flp-In *SLC25A46* knockout cells using quantitative PCR (qPCR; Figure 2E). Thus the knockout of SLC25A46 stabilizes MFN1 and MFN2 on mitochondria because of decreased degradation of MFN1 and MFN2.

SLC25A46 does not function in mitochondrial phospholipid biogenesis and trafficking pathways

Because the MICOS complex has been implicated in lipid biogenesis and trafficking and SLC25A46 yeast homologue Ugo1 was believed to regulate the local lipid composition of the OM

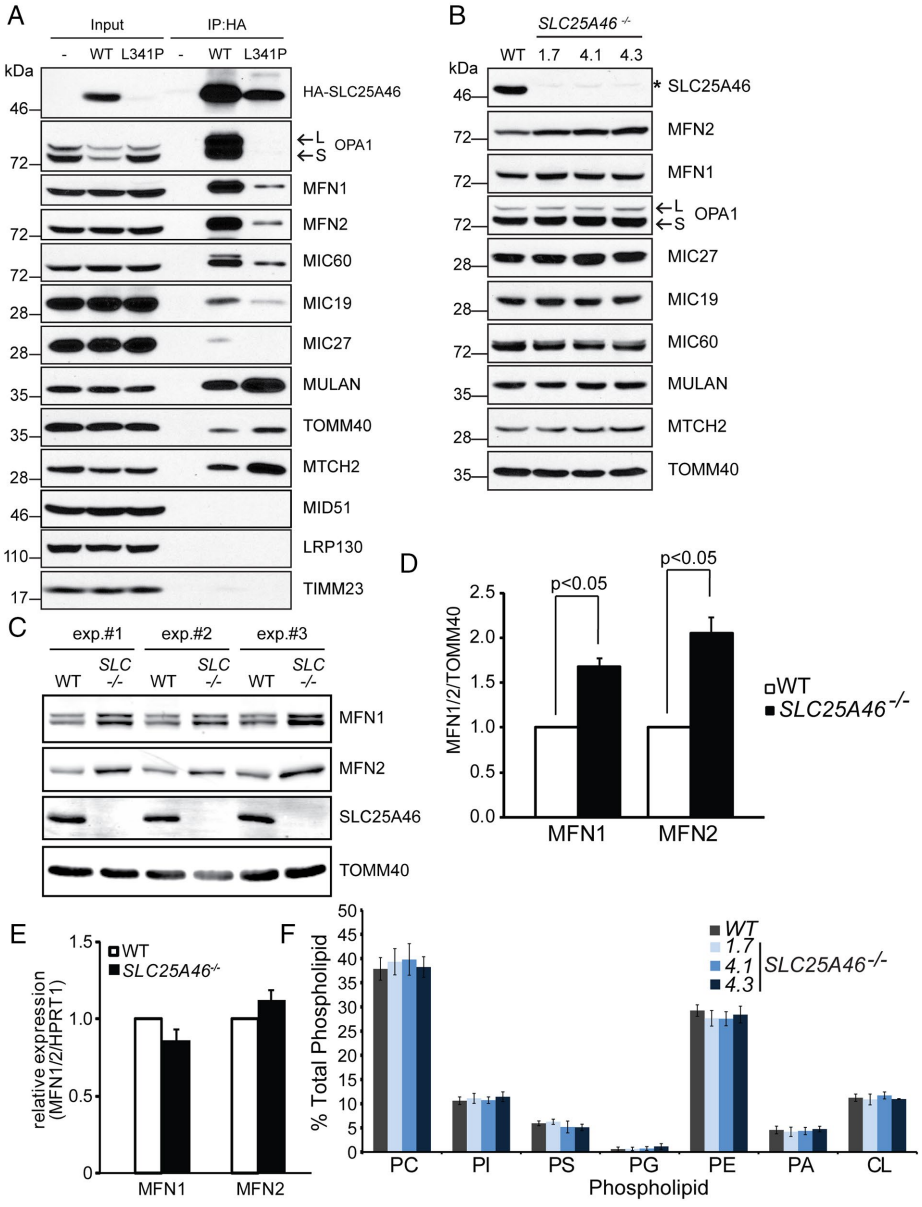

FIGURE 2: SLC25A46 interacts with proteins important for mitochondrial biogenesis and morphology. (A) IP with the HA antibody from whole-cell extracts of HEK293T or stable HEK293T cells expressing 2xHA-SLC25A46 WT or 2xHA-SLC25 L341P. Cells were cross-linked with dithiobis(succinimidyl propionate) before lysis. Samples were analyzed with the indicated antibodies. Input samples represent 2% of the material used for the IP. Short (S) and long (L) forms of OPA1 are marked. (B) Steady-state level of SLC25A46 interaction partners in HCT116 WT or *SLC25A46* knockout (*SLC25A46*$^{-/-}$) cells was determined. Mitochondria from each cell line were isolated, solubilized, separated by SDS–PAGE, and analyzed with immunoblotting. Three different single-cell knockout clones designated 1.7, 4.1, and 4.3, using two different gRNAs. The asterisk marks a nonspecific band of the antibody. (C) Steady-state levels of MFN1 and MFN2 in HEK293 T-REx Flp-In WT, and *SLC25A46*$^{-/-}$ cells were measured in three independent experiments. Mitochondria from each cell line were isolated, solubilized, separated by SDS–PAGE, and analyzed with immunoblotting. TOMM40 was included as a loading control. (D) Densitometric analysis of C. Results are shown as mean ± SEM of three independent experiments. *t* test, $p < 0.05$. (E) Analysis of *MFN1* and *MFN2* expression in HEK293 T-REx Flp-In WT and *SLC25A46*$^{-/-}$ cells by qPCR (mean ± SEM, $n = 3$). (F) Knockout of *SLC25A46* does not alter the phospholipid composition of mitochondria. Phospholipids were extracted from 0.75 mg of mitochondria in the cell lines as in B, separated by thin-layer chromatography, and visualized using molybdenum blue staining. Scanned images were analyzed using Quantity 1 software, and the relative abundance of each phospholipid was calculated as percentage of the total phospholipid in each sample (mean ± SEM, $n = 3$). CL, cardiolipin; PA, phosphatidic acid; PC, phosphatidylcholine; PE, phosphatidylethanolamine; PI, phosphatidylinositol; PG, phosphatidylglycerol; PS, phosphatidylserine.

(Hoppins *et al.*, 2009; Anton *et al.*, 2011), we assessed whether mitochondrial lipid levels were altered in *SLC25A46*$^{-/-}$ cells. Total phospholipid content in mitochondria was analyzed, and no differences were detected (Supplemental Figure S3A). The lipid profile was assessed using thin-layer chromatography (Supplemental Figure S3B), and the individual phospholipids were quantitated (Figure 2F). The profile of the individual lipids was not different in the *SLC25A46*$^{-/-}$ cell lines than in WT HCT116 cells. Thus SLC25A46 does not play a direct role in lipid biogenesis or lipid trafficking.

The abundance of MFN1 and MFN2 is increased in cells lacking SLC25A46

Because we observed higher steady-state levels of MFN1 and MFN2 in cells lacking SLC25A46, we investigated the assembly of these proteins. Because SLC25A46 is highly expressed in neuronal tissue and mutant SLC25A46 impairs neuronal function (Haitina *et al.*, 2006; Abrams *et al.*, 2015; Wan *et al.*, 2016), we used short hairpin RNAs (shRNAs) to knock down SLC25A46 in LAN5 cells (Figure 3, A and B). As observed in HCT116 and HEK293 T-REx Flp-In *SLC25A46*$^{-/-}$ cells, the steady-state levels of MFN1 and MFN2 were slightly elevated after SLC25A46 knockdown (Figure 3A). This led to an elevated abundance of MFN1 and MFN2 complexes in cells lacking SCL25A46 when isolated mitochondria were solubilized in digitonin and separated by BN-PAGE (Figure 3B). Again, we did not observe any marked changes in the expression of transcripts for MFN1 and MFN2 (Figure 3C). We obtained similar results in HCT116 *SLC25A46*$^{-/-}$ cells (Supplemental Figure S4).

To determine whether the enhanced oligomerization states of MFN1 and MFN2 lead to hyperfused mitochondria, we knocked down SLC25A46 in LAN5 cells by RNA interference (RNAi) and visualized mitochondria by immunofluorescence staining using an antibody against the matrix protein Mortalin and the OM protein TOMM20. As expected, mitochondria appeared elongated and hyperfused in cells with SLC25A46 knock down, as reported previously (Figure 3D; Abrams *et al.*, 2015; Janer *et al.*, 2016; Wan *et al.*, 2016). To confirm that the mitochondrial network was indeed hyperfused in SLC25A46-knockdown cells, we quantitated the mitochondrial network (Figure 3E). In cells that lacked SLC25A46, the network consisted of ~65% hyperfused and ~30% normal mitochondria. In contrast, the control cells had a network with ~70% normal and

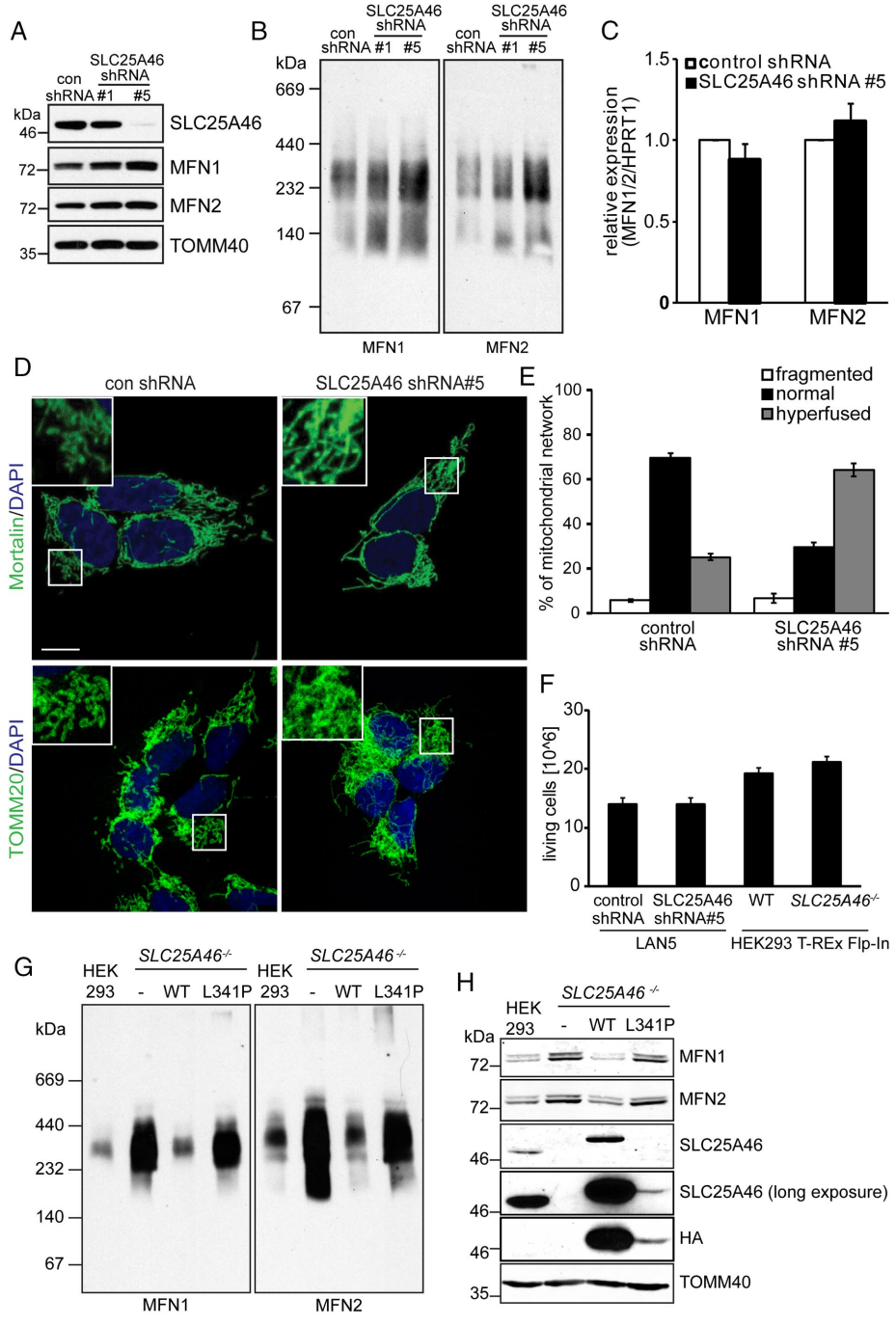

FIGURE 3: SLC25A46 levels affect the steady-state levels and assembly of MFN1 and MFN2. (A) The oligomerization of MFN1 and MFN2 was determined in isolated mitochondria from LAN5 cell lines in which SLC25A46 was knocked down with different shRNA constructs after doxycycline induction using BN-PAGE and immunoblotting. (B) The steady-state levels of the indicated proteins were determined using the same mitochondrial extracts loaded on BN-PAGE in A. (C) Analysis of *MFN1* and *MFN2* expression in LAN5 cells in which SLC25A46 was knocked down with a specific shRNA construct by qPCR (mean ± SEM, $n = 3$). (D) The mitochondrial network in LAN5 cell lines in which SLC25A46 was knocked down after doxycycline induction was investigated by immunofluorescence staining using an antibody against the matrix protein Mortalin or OM protein TOMM20. 4′,6-Diamidino-2-phenylindole was used to stain the nucleus. Scale bar, 10 µm. (E) Quantification of the mitochondrial network from D. For each experiment, 100 cells were counted (mean ± SEM, $n = 3$). (F) Live cells were quantitated using a trypan blue assay in the LAN5 and HEK294 T-REx Flp-In lines. An equal number of cells from each line was plated, and then live cells were counted after 4 d. The expression of SLC25A46 in LAN5 was knocked down for 2 wk before the experiment. Data represent mean ± SEM. ($n = 3$). (G) As in A, but the oligomerization of MFN1 and MFN2 was analyzed in HEK293 T-REx Flp-In cells lacking SLC25A46. SLC25A46 knockout was rescued by expressing 2xHA-SLC25A46 WT or L341P for 48 h after induction with 10 ng/ml doxycycline. (H) Lysates from G were separated by SDS–PAGE and the steady-state levels of indicated proteins investigated by immunoblot. 2xHA-SLC25A46 and endogenous SLC25A46 were detected with anti-SLC25A46; a longer exposure to detect HA-SLC25A46 L341P of the panel was included. A panel with anti-HA was also included to detect expressed HA-SLC25A46 WT and L341P.

~25% hyperfused mitochondria. Thus the mitochondrial network in LAN5 cells that lack SLC25A46 is aberrant, marked with a hyperfused network.

MFN1 and MFN2 oligomerization can be confirmed by cross-linking with a cysteine–cysteine cross-linker, which yields high–molecular weight complexes in SDS gels. In *SLC25A46*$^{-/-}$ HCT116 or LAN5 SLC25A46 knockdown cells, an increased abundance of MFN1 and MFN2 oligomers was detected by cross-linking (Supplemental Figure S5, A and B). Our results support the observation that decreased SLC25A46 expression leads to hyperfused mitochondria (Figure 3, D and E; Abrams *et al.*, 2015; Wan *et al.*, 2016), which correlates with increased steady-state levels and oligomerization of MFN1 and MFN2 complexes in hyperfused mitochondria.

Because hyperfused mitochondria might influence cell viability, we analyzed the cell growth of HEK293 T-REx Flp-In *SLC25A46*$^{-/-}$ and LAN5 cells in which SLC25A46 expression was silenced by a specific shRNA (Figure 3F). However, changes in cell viability were not detected in these lines (Figure 3F). Our results contrast with a recent study by Janer *et al.* (2016) in which fibroblast lines derived from a patient or knocked down for SLC25A46 showed increased cell senescence.

Expression of SLC25A46 L341P does not rescue elevated MFN1 and MFN2 levels in cells lacking *SLC25A46*

Next we analyzed whether mutant SLC25A46 L341P is able to rescue the phenotype in SLC25A46 knockout cells because our previous studies indicated that the L341P mutation destabilized SLC25A46, causing hyperfused mitochondria and lethal PCH (Wan *et al.*, 2016). SLC25A46 was deleted in HEK 293 T-REx Flp-In cells, and doxycycline-inducible 2xHA-SLC25A46 WT or L341P was introduced. Isolated mitochondria from these cell lines were

subjected to SDS- and BN-PAGE as in Figure 3, A and B. Again, MFN1 and MFN2 showed increased steady-state levels and oligomerization when SLC25A46 was knocked out (Figure 3, G and H). Whereas the induction of 2xHA-SLC25A46 WT rescued the knockout, the induction of 2xHA-SLC25A46 L341P failed and instead increased steady-state levels, and oligomerization of MFN1 and MFN2 prevailed (Figure 3, G and H). Note that expression of the HA-SLC25A46 proteins was confirmed by immunoblotting with an anti-HA antibody. In addition, anti-SLC25A46 was used to detect expression of endogenous SLC25A46 and HA-tagged SLC25A46; because 2xHA-SLC25A46 L341P is rapidly degraded, this panel was overexposed to verify that 2xHA-SLC25A46 L341P was present (Figure 3H). Thus cells expressing SLC25A46 L341P have a phenotype identical to that of SLC25A46 knockout.

SLC25A46 L341P is not stable

Because rapid turnover of a specific mitochondrial OM protein is an unexpected molecular basis for a disease, we investigated this degradation pathway in detail. We transiently transfected HEK293T cell lines with constructs that expressed SLC25A46 WT or L341P mutant protein containing a 2xHA epitope at the N-terminus. We treated cells with cycloheximide to block cytosolic translation and removed aliquots in a time-course chase (Figure 4A). SLC25A46 was detected with an anti-HA antibody. Mitochondrial OM protein TOMM40 was included as a control. The abundance of SLC25A46 was quantitated by densitometry (Figure 4B). Whereas TOMM40 and WT SLC25A46 were stable during the chase, SLC25A46 L341P was not detected, except when the blot was overexposed relative to WT SLC25A46. Note that the apparent increase in abundance of SLC25A46 at the 40- and 60-min time points is unexpected but likely indicative of the normal variability associated with the stable protein in these types of experiments; we observed this previously (Hwang *et al.*, 2007). To determine whether different amino acid substitutions were tolerated, changes including a basic (arginine, R), acidic (glutamate, E), and conservative hydrophobic (valine, V) substitution were made to SLC25A46 at position 341, and the stability was tested as in Figure 4A (Figure 4C). Again, the arginine and glutamate substitutions markedly reduced stability, similar to the proline mutation, and the conservative valine substitution also decreased the stability of SLC25A46, but the protein was detectable upon a shorter exposure of the film. Therefore the mutation at position 341 strongly decreases the stability of SLC25A46.

Mutations in SLC25A46 were also identified in patients with optic atrophy spectrum disorder (Abrams *et al.*, 2015). These mutations were associated with defects in mitochondrial morphology but the fate of mutant SLC25A46 protein was not determined. Two mutations, P333L and R340C, were near L341P and localized to the putative fifth membrane-spanning domain, based on homology with mitochondrial carriers (Wan *et al.*, 2016). As in Figure 4C, the abundance of these proteins was determined using cycloheximide-chase studies (Figure 4D). SLC25A46 R340C was detected, but L341P and P333L variants were identified only when the blot was exposed for a longer time. The patient with the P333L mutant died at 15 wk of life, whereas the patient with the R340C mutation was 51 yr old at the time of the study (Abrams *et al.*, 2015). Thus rapid turnover of SLC25A46 during development is likely associated with the early onset of death.

To determine whether the rapid degradation of SLC24A46 L341P was a result of the mutant protein failing to reach its native conformation in the OM after import, we imported radiolabeled SLC25A46 WT, L341P, and R340C into isolated mitochondria and treated half of the sample with a low amount of trypsin to perform

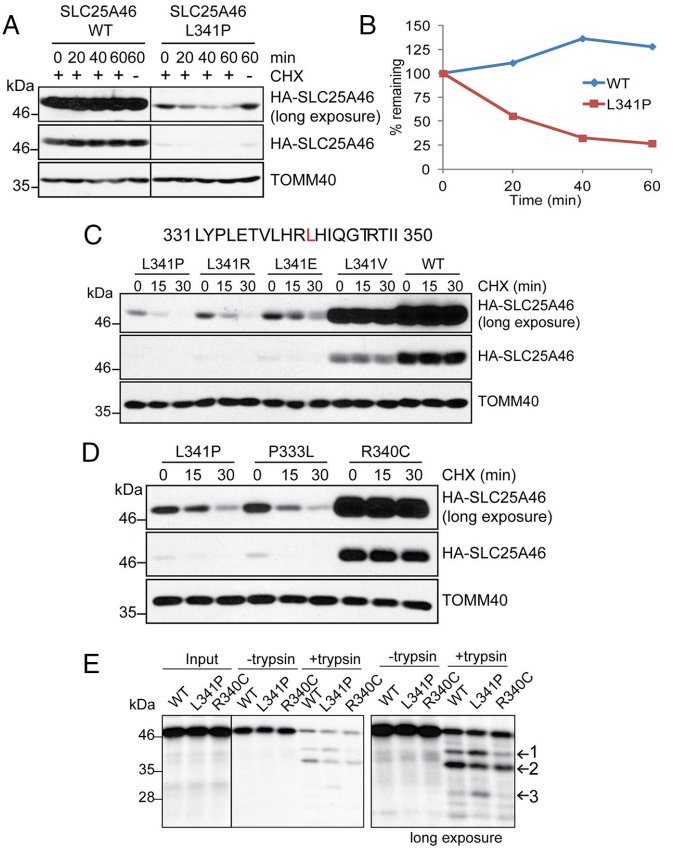

FIGURE 4: SLC25A46 L341P is very unstable in cultured cells and does not reach its native conformation. (A) The half-life of WT SLC25A46 or SLC25A46 L341P was determined by cycloheximide (CHX)-chase experiments. HEK293T cells were transiently transfected with constructs for 2xHA-SLC25A46 WT or 2xHA-SLC25A46 L341P. At 24 h posttransfection, CHX was added, and samples were taken at the indicated time points. The mitochondria were isolated and analyzed with antibodies against the HA tag and control TOMM40. (B) Densitometry of immunoblots from A. (C) As in A, constructs were generated with the indicated mutations at position 341. (D) As in A, constructs were generated with the indicated mutations at positions 341, 333, and 340. (E) Radiolabeled 2xHA-SLC25A46 WT, L341P, and R340C were imported for 10 min into mitochondria isolated from HEK293 T-REx Flp-In cells. After import, half of the sample was treated with 1.25 µg/ml trypsin for 15 min on ice, and inserted proteins were recovered in the pellet after alkali extraction. As a control, the other half was incubated for 15 min on ice, followed by alkali extraction. All samples were resolved by SDS–PAGE and visualized by autoradiography. Arrows labeled 1–3 indicate different cleavage products that were prominent in the panel that was exposed for a longer time.

limited proteolysis. Membrane insertion was confirmed by alkali extraction (Figure 4E). In the absence of trypsin treatment, all three proteins were imported to the same extent. Comparison of the cleavage products after limited proteolysis showed that the three proteins had differing cleavage patterns. Three prominent degradation products were detected and labeled on the panel with the longer exposure. SLC25A46 WT and R340C had a prominent cleavage product at position 2 and minor product at position 1, with the exception that R340C had less of these products than WT. In contrast, SLC25A46 L341P had an additional cleavage product at position 3 that was more prominent than for WT and R340C. Thus we conclude that SLC25A46 L341P is imported

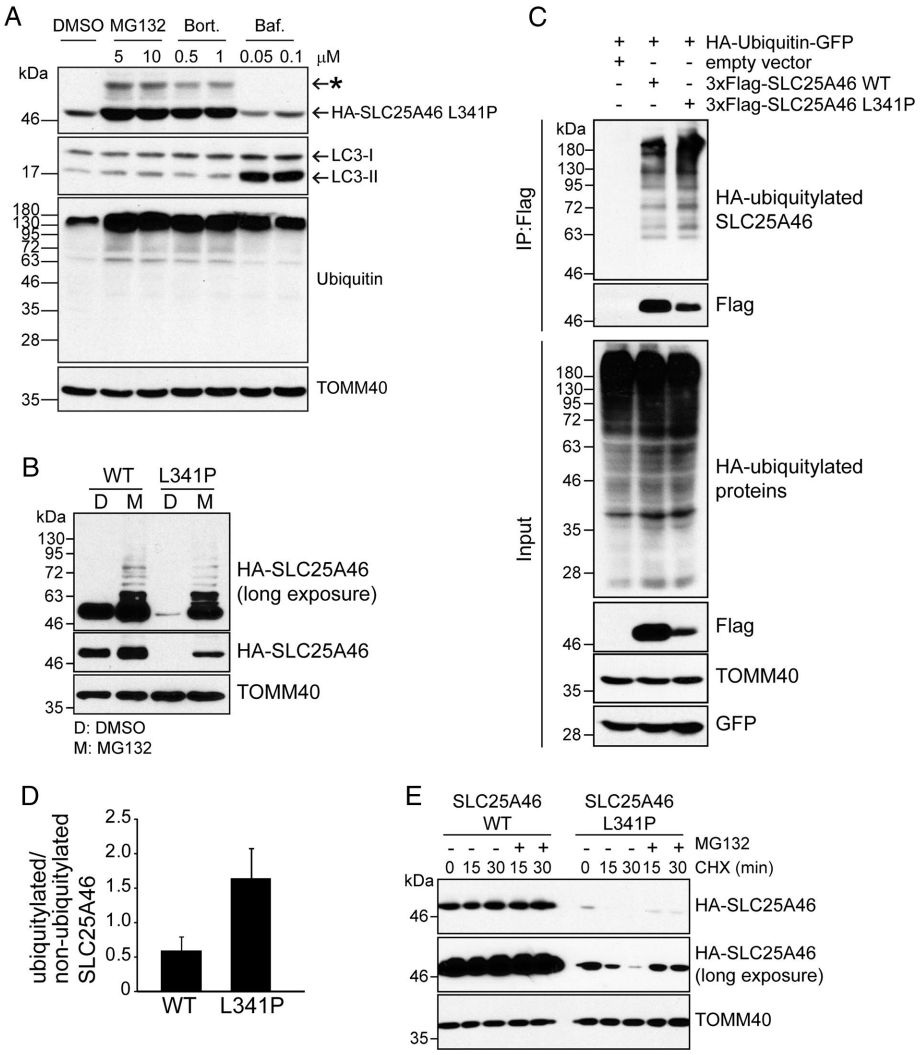

FIGURE 5: SLC25A46 L341P is polyubiquitylated and degraded by the proteasome. (A) HEK293 T-REx Flp-In cells expressing 2xHA-SLC25A46 L341P were treated with MG132, bortezomib, bafilomycin A1, or DMSO (0.1%) for 6 h. Cells were lysed, and total extracts were analyzed by SDS–PAGE. Antibodies against LC3 and ubiquitin were included as controls to verify inhibition of autophagy and protein degradation, respectively. TOMM40 served as loading control. The asterisk marks monoubiquitylated 2xHA-SLC25A46 L341P. (B) SLC25A46 L341P accumulates on mitochondria upon proteasome inhibition. HEK293T cells were transfected as in A and then treated with 10 μM MG132 (M) or control DMSO (D) for 6 h. Mitochondria were isolated and lysed; HA-tagged SLC25A46 L341P was detected by immunoblotting. (C) Ubiquitylated SLC25A46 WT or L341P was immunoprecipitated under denaturing conditions with a Flag antibody from cells transiently expressing HA-ubiquitin-GFP and 3xFlag-SLC25A46 WT or L341P. Ubiquitin was detected with an anti-HA antibody. GFP cleaved from HA-ubiquitin served as transfection control, and TOMM40 was included as a loading control. (D) The ratio between ubiquitylated and nonubiquitylated SLC25A46 WT and L341P was determined after densitometric analysis of both proteins pools of C. Mean ± SEM $n = 3$. (E) Proteasome inhibition blocks the rapid degradation of SLC25A46 L341P in mitochondria. HEK293T were transiently transfected with constructs for 2xHA-SLC25A46 WT or L341P for 24 h and then harvested before (0) and 15 or 30 min after the addition of cycloheximide. Mitochondria were isolated and analyzed by SDS–PAGE and immunoblotting. To block proteasome-dependent degradation, 25 μM MG132 was added at the time as cycloheximide addition.

normally but does not reach the native conformation, resulting in rapid degradation. That SLC25A46 L341P does not fold into its final conformation is also supported by the observation that SLC25A46 L341P displayed a different distribution pattern in the glycerol gradients and BN-PAGE than did WT SLC25A46 (Figure 1, A and C).

SLC25A46 L341P is polyubiquitylated and degraded by the proteasome

The strong interaction of SLC25A46 L341P with MULAN implies that mutant SLC25A46 may be rapidly degraded by the UPS (Figure 2A). However, it has been suggested that mitochondrial OM proteins are turned over only by mitophagy with the ultimate removal of the entire organelle (Ling and Jarvis, 2013). Therefore we investigated the turnover process in more detail. Cells expressing SLC25A46 L341P were treated with the two proteasome inhibitors MG132 and bortezomib and with the late-phase autophagy inhibitor bafilomycin A1 (Figure 5A). Because MG132 at a 10-fold higher concentration can also inhibit the proteolytic calpains and cathespins (Tsubuki *et al.*, 1996; Kisselev and Goldberg, 2001), bortezomib, which is proteasome specific, was also used (Moore *et al.*, 2008). The steady-state level of SLC25A46 L341P was increased only when the cells were treated with MG132 or bortezomib (Figure 5A). Proteins that are degraded by the proteasome are typically ubiquitylated, resulting in a decreased mobility in SDS gels. A fraction of SLC25A46 L341P displayed reduced mobility after proteasome inhibition, suggesting ubiquitylation (Figure 5A; the monoubiquitylated fraction is marked with an asterisk). In contrast, SLC25A46 L341P was not stabilized upon bafilomycin A1 treatment, although the autophagy marker LC3-II accumulated, indicating autophagy was indeed inhibited (Figure 5A). When we analyzed mitochondria from HEK293T cells that were transiently transfected with HA-SLC25A46 WT or L341P mutant, we found that MG132 treatment again markedly stabilized HA-SLC25A46 L341P, whereas HA-SLC25A46 WT was only slightly stabilized (Figure 5B). Moreover, a fraction of the SLC25A46 WT and L341P from MG132-treated cells also showed decreased mobility after increased exposure, supporting ubiquitylation of the proteins (Figure 5B). In HeLa cells transiently transfected with HA-tagged SLC25A46 WT or L341P, mutant SLC25A46 was barely detectable (Supplemental Figure S6) and localized to mitochondria and the cytosol; however, no large aggregates were observed. In comparison, SLC25A46 WT was abundant and exclusively localized to mitochondria. When the cells were treated with MG132, SLC25A46 L341P and WT accumulated on mitochondria and in the cytosol. We conclude that SLC25A46 L341P does not form large aggregates but is imported into mitochondria and then is quickly retrotranslocated to the cytosol due to instability. WT SLC25A46 follows a similar pathway but with slower kinetics.

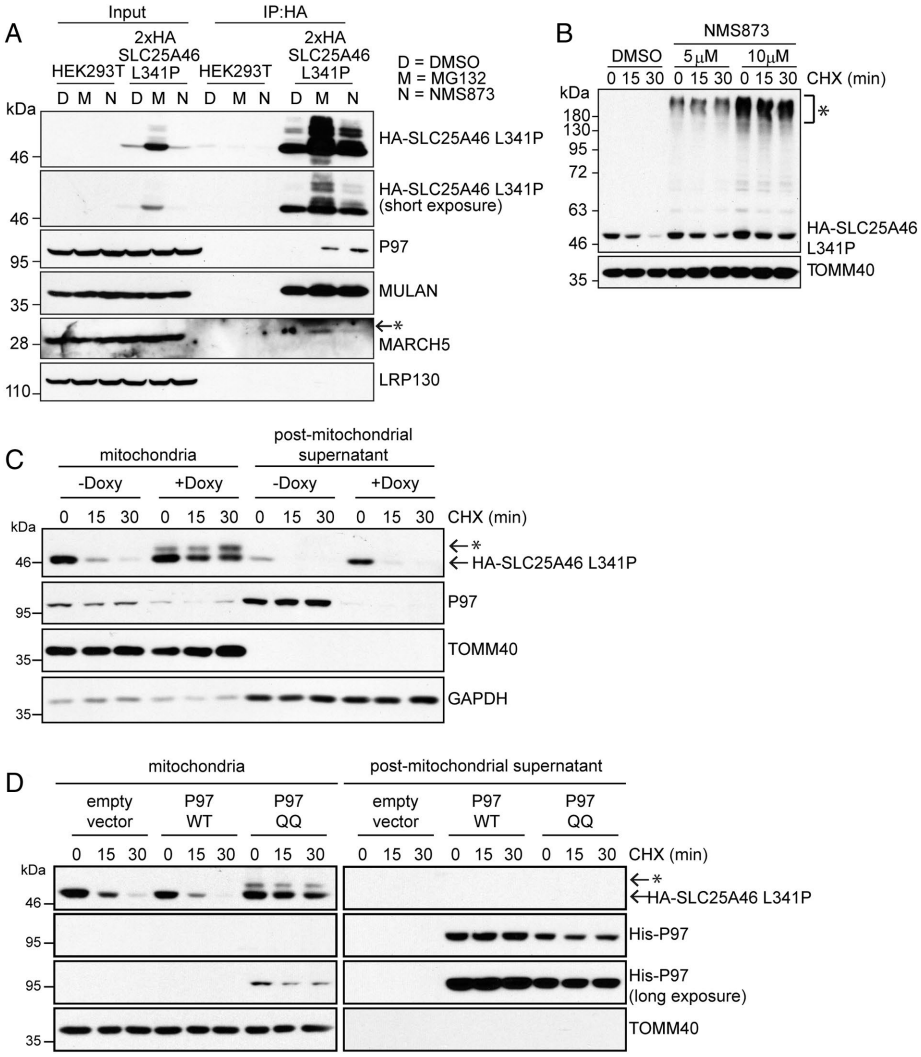

FIGURE 6: Rapid turnover of SLC25A46 L341P strongly depends on P97. (A) SLC25A46 binds to P97, MARCH5, and MULAN. Stable HEK293T cells expressing 2xHA-SLC25A46 L341P were treated with DMSO (vehicle control), 25 μM MG132 (M), or 5 μM NMS873 (N) for 3 h before cell lysis. Cells were lysed in digitonin, and SLC25A46 was immunoprecipitated from whole-cell extracts with anti-HA antibody. Antibodies against HA, P97, MULAN, and matrix control LRP130 were used for immunoblotting. Input samples correspond to 2% of the amount of lysate used for the IP. The asterisk marks an unspecific signal in the IP lanes for MARCH5. (B) Inhibition of P97 alters degradation of SLC25A46 L341P. The same cells as in A were treated with DMSO and 5 or 10 μM NMS873 in combination with CHX. At the indicated times, cells were harvested and mitochondria were isolated. SLC25A46 L341P degradation was detected by immunoblotting, and TOMM40 was included as a loading control. The asterisk marks polyubiquitylated species. (C) HEK293T cells stably expressing doxycycline (Doxy)-inducible shRNA targeting P97 were transfected with a construct for 2xHA-SLC25A46 L341P. After 24 h, cells were treated with CHX, and samples were removed at the indicated times. Cells were separated into a mitochondrial pellet and a postmitochondrial supernatant; equal amounts of protein from each fraction were analyzed by SDS–PAGE and immunoblotting. Doxycycline treatment was started 24 h before transfection and maintained during the analysis. The asterisk marks monoubiquitylated SLC25A46. (D) The half-life of SLC25A46 L341P was determined in HEK293T cells transiently expressing 2xHA-SLC25A46 L341P in combination with WT P97, active-site-mutant P97-QQ, or empty vector. Cells were treated with CHX and analyzed as described in C. The asterisk marks monoubiquitylated SLC25A46.

To confirm SLC25A46 ubiquitylation, we transiently transfected cells with Flag-tagged SLC25A46 WT or L341P, as well as with a construct for HA-tagged ubiquitin-GFP (and as a control, an empty vector; Figure 5C). SLC25A46 from lysates was immunoprecipitated with anti-Flag followed by immunoblotting with anti-HA. As expected, SLC25A46 was ubiquitylated, with the mutant L341P possessing greater modification (Figure 5, C and D).

To verify the UPS involvement in the turnover of SLC25A46, were subjected cells transiently transfected with SLC25A46 WT or L341P to a cycloheximide chase in the presence of the MG132 to assess SLC25A46 stability (Figure 5E). SLC25A46 WT was stable, whereas SLC25A46 L341P was present at lower levels, but degradation was detected upon longer exposure to film. The addition of MG132 stabilized the SLC25A46 L341P, confirming that the proteasome degraded mutant L341P. TOMM40 was stable and included as a loading control. Thus SCL25A46 L341P in the mitochondrial OM is extensively ubiquitylated and degraded by the proteasome, independently of mitophagy.

MULAN and MARCH5 coordinately ubiquitylate SLC25A46 L341P, and P97 mediates the degradation of SLC25A46

We determined the components that mediate SLC25A46 turnover by taking advantage of inhibitors, mutants, and RNAi silencing. When HEK293T cells stably expressing SLC25A46 L341P were treated with the proteasome inhibitor MG132 (M) or P97 inhibitor NMS873 (N; Magnaghi *et al.*, 2013), coIP assays revealed a robust interaction of SCL25A46 L341P with MULAN and a weaker interaction with P97 (Figure 6A). A strong interaction with MARCH5 was not detected, because MARCH5 failed to coimmunoprecipitate with SCL25A46 L341P (Figure 6A). Note that immunoblots with the antibody for endogenous MARCH5 yield some background, and a nonspecific band that migrates at a higher molecular weight than MARCH5 was detected (marked with an asterisk in Figure 6A).

We followed this investigation with cycloheximide-chase experiments to stop cytosolic translation and investigated SLC25A46 L341P stability under conditions that decreased proteolysis (Figure 6, B–D). Aliquots were removed before cycloheximide treatment and 15 and 30 min posttreatment, and mitochondria lysates were subjected to immunoblotting. Treatment with NMS873 to inhibit P97 before the cycloheximide chase resulted in SLC25A46 L341P accumulating in large–molecular mass complexes (marked with an asterisk), indicating an accumulation of polyubiquitylated SLC25A46 L341P mutant on mitochondria (Figure 6B). We do not expect that this fraction of SLC25A46 (marked with an asterisk) is a nonspecific aggregate because 1) the high–molecular mass form of SLC25A46 was not detected when the cells were mock treated with dimethyl sulfoxide (DMSO); 2) the

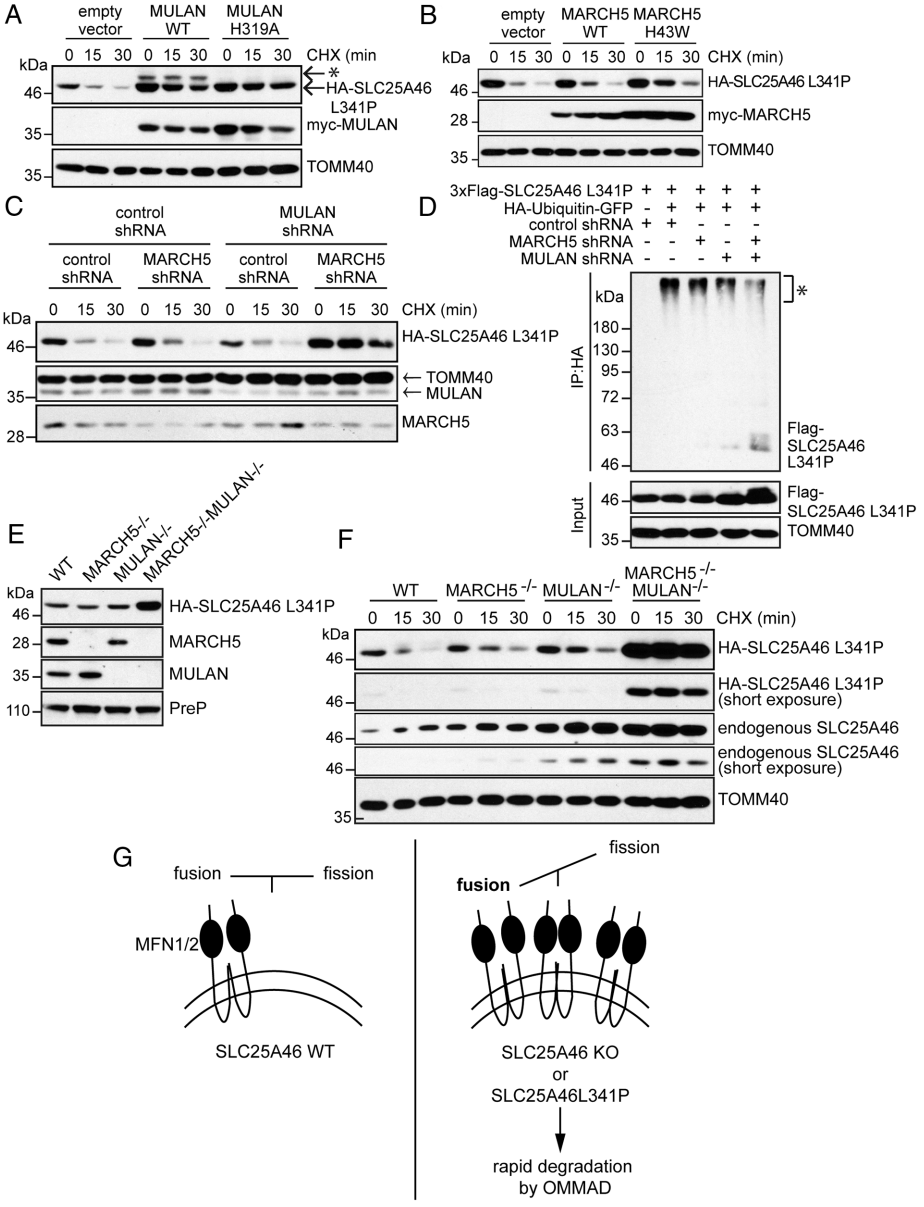

FIGURE 7: MARCH5 and MULAN mediate SLC25A46 L341P ubiquitylation and degradation. (A) Increased half-life of SLC25A46 L341P by overexpressing the RING-finger mutant MULAN H319A. A stable cell line expressing 2xHA-SLC25A46 L341P was transiently transfected with an empty vector, WT MULAN, or MULAN H319A and treated with CHX for indicated time points. Mitochondria were isolated, and MULAN was detected with an anti-myc antibody. The asterisk marks monoubiquitylated SLC25A46. (B) As in A, with the exception that the cells were transiently transfected with WT MARCH5 or the RING-mutant MARCH5 H43W. (C) HEK293T cells stably expressing Doxy-inducible control shRNA or a shRNA targeting MULAN were transfected with constructs for control shRNA or shRNA targeting MARCH5 and 2xHA-SLC25A46 L341P. Doxycycline (1 μg/ml) was added during transfection. After 48 h, CHX was added, and cells were harvested just before CHX addition (0) and at 15 and 30 min. Mitochondria were isolated and analyzed by SDS–PAGE and immunoblotting. (D) As in C, but cells were transfected with 3xFlag-SLC25A46 L341P and HA-Ubiquitin-GFP. After treatment of the cells with 25 μM MG132 for 3 h, HA-tagged ubiquitylated proteins were immunoprecipitated under denaturing conditions with anti-HA. Ubiquitylated 3xFlag-SLC25A46 L341P was detected with an anti-Flag antibody. The asterisk marks polyubiquitylated species. TOMM40 is a loading control. (E) Determination of SLC25A46 L341P abundance in HEK293 T-REx Flp-In WT, MARCH5, MULAN, or MARCH5/MULAN knockout cells. Cells were transfected with a 2xHA-SLC25A46 L341P construct; mitochondria from the cell lines were isolated, solubilized, separated by SDS–PAGE, and analyzed by immunoblotting. PreP was included as a loading control. (F) As in E, with CHX treatment for the indicated times. Cells were harvested at each time point, and mitochondria were isolated. SLC25A46 L341P and endogenous SLC25A46 were detected by immunoblotting, and TOMM40 was included as a loading control. (G) Under physiological expression of WT SLC25A46, the levels of MFN1, MNF2, and dimers are kept constant so as not to disturb the fine balance between fission and fusion, which is important for development and survival (left). However, when the gene SLC25A46 is disrupted by deletions or the gene product destabilized by point mutations like L341P, which is quickly degraded by OM–associated degradation, MFN1 and MFN2 dimers accumulate on the OM and shift the balance towards fusion. This leads to pontocerebellar hypoplasia and early death (right).

samples were prepared for SDS–PAGE with a sample buffer that contained SDS, resulting in the expected solubilization of SLC25A46; and 3) SLC25A46 prepared in SDS-containing sample buffer is not observed in the stacking gel, and the SLC25A46 fraction at the top of the gel (marked with an asterisk) entered into the separating gel. P97 protein expression was decreased using a doxycycline-inducible shRNA system (Figure 6C). Decrease in P97 protein levels correlated with increased stability of SLC25A46 L341P on mitochondria and a slight increase in the stability of a cytosolic pool. This supports a pathway in which SLC25A46 is first inserted into the mitochondrial OM and then subsequently degraded. In addition, expression of the active-site P97-QQ mutant mirrored the shRNA induction (Figure 6D), in which SLC25A46 L341P was stabilized on the mitochondrial membrane; moreover, a monoubiquitylated form of SLC25A46 L341P (marked with an asterisk) was detected, and a fraction of the P97-QQ mutant associated with the SLC25A46 mutant on mitochondria. In contrast, overexpression of active P97 did not increase accumulation of mutant SLC25A46 (Figure 6D). Note that in Figure 6C with anti-P97, a fraction of the P97 pool was detected in the mitochondrial fraction, which likely reflects a pool of P97 that might be engaged in SLC25A46 degradation. Similarly, a small fraction of the P97-QQ mutant was identified in the mitochondrial fraction; this pool may be larger because the anti-histidine antibody is not as robust as the P97 antibody.

We manipulated MULAN expression. Overexpressing MULAN resulted in increased monoubiquitylation of SLC25A46 L341P (marked with an asterisk). However, "ligase-dead" MULAN H319A increased SLC25A46 L341P stability but lacked ubiquitylation (Zhang *et al.*, 2008; Figure 7A).

Initially, we anticipated that overexpression of WT MULAN would result in increased turnover of SLC25A46 L341P, similar to the conditions of the empty vector control. However, overexpression of MULAN is likely not well tolerated by cells because reports indicate that overexpression of WT MULAN inhibits cell growth and causes cell death (Zhang *et al.*, 2008; Bae *et al.*, 2012). Therefore we interpret this result as indicating that increased abundance of active MULAN causes increased degradation of key proteins required for cell survival, such as Akt (Bae *et al.*, 2012), and long-term MULAN overexpression leads to apoptosis via activation of caspases (Zhang *et al.*, 2008). Indeed, long-term overexpression of MULAN leads to cell death in these experiments. We conclude that under apoptotic conditions, the quality control pathway for proteins such as SLC25A46 L341P is not working efficiently and therefore SLC25A46 turnover is not as robust as in the case of expression of the empty vector. In addition, a similar result was found with the endoplasmic reticulum (ER) ubiquitin ligase HRD1. Overexpression of the mutant HRD1 failed to degrade nonsecreted immunoglobulin κ light chain (Ig κ LC), but overexpression of WT HRD1 also inhibited degradation of nonsecreted Ig κ LC (Okuda-Shimizu and Hendershot, 2007). Thus the results with HRD1 mirror those with overexpression of WT MULAN.

We used a similar approach with manipulation of MARCH5 expression. Transient transfection of WT MARCH5 resulted in degradation of SLC25A46 L341P similar to the transfection with an empty vector (Figure 7B). In contrast, transfection with the ring-domain mutant MARCH5 H43W resulted in stabilization of SLC25A46 L341P to a minor extent (Karbowski *et al.*, 2007).

Using the shRNA approach to decrease MULAN and MARCH5 expression, we found that SLC25A46 L341P was markedly stabilized when the expression of both was reduced (Figure 7C). To confirm ubiquitylation of SLC25A46 L341P specifically by MULAN and MARCH5, we combined Flag-tagged SLC25A46 L341P and HA-ubiquitin–green fluorescent protein (GFP) transfection with the MULAN and MARCH5 RNAi treatment as in Figure 5C. Again, knockdown of both MULAN and MARCH5 shifted the pool of polyubiquitylated SLC25A46 L341P to a cohort that was less ubiquitylated (Figure 7D, asterisk). As in Figure 6B, we do not expect the fraction of Flag-SLC25A46 L341P that migrates at a high molecular mass (asterisk) to be a nonspecific aggregate because this fraction was not detected in the sample treated with the control shRNA. In addition, on the basis of the assay, we first immunoprecipitated proteins that were HA-ubiquitylated and then blotted for Flag-SLC25A46 L341P with anti-Flag. Therefore the fraction of Flag-SLC25A46 L341P that migrates at a high molecular mass (asterisk) is polyubiquitylated.

To verify the role of MULAN and MARCH5 on the degradation of SLC25A46 L341P, we generated HEK293 T-REx Flp-In *MULAN*$^{-/-}$, *MARCH5*$^{-/-}$, and *MULAN*$^{-/-}$/*MARCH5*$^{-/-}$ cell lines and analyzed the abundance of the SLC25A46 L341P when transiently transfected (Figure 7E). Again, only in the absence of MARCH5 and MULAN were SLC25A46 L341P steady-state levels increased in comparison to the single E3 ligase knockouts. As observed in the shRNA approach, SLC25A46 L341P was stabilized markedly when both E3 ligases were knocked out in the HEK293 T-REx Flp-In cell lines (Figure 7F). Single knockout of MULAN or MARCH5 had little effect on the half-life of SLC25A46.

The Cullin RING ligase family does not ubiquitylate SLC25A46 L341P

Another class of E3 ubiquitin ligases that may play a role in degrading SLC25A46 L341P is the Cullin RING ligase (CRL) family (Supplemental Figure S7). Previously SLC25A46 was identified as a potential CRL3 substrate (Emanuele *et al.*, 2011). The small molecule MLN4924, which inhibits the NEDD8-activating enzyme and thereby prevents the activation of Cullin RING ligases, was added to cells before the cycloheximide chase (Soucy *et al.*, 2009). SLC25A46 L341P was not stabilized under these conditions. However, the inhibitor was active because it prevented the neddylation of Cul4a by Nedd8 (Brownell *et al.*, 2010). Thus, of the ubiquitin ligases, MARCH5 and MULAN coordinate SLC25A46 degradation and seem to have redundant functions.

DISCUSSION

SLC25A46 is a regulator of mitochondrial dynamics and morphology. SLC25A46 interacts with fusion regulators MFN1, MFN2, and OPA1. In cells with decreased SLC25A46, the abundance of MFN1and MFN2 was elevated, and the pool shifted to that of an assembled oligomeric complex; this correlates with knockdown of SLC25A46 resulting in hyperfused mitochondria (Figure 3E; Abrams *et al.*, 2015; Wan *et al.*, 2016). Whereas SLC25A46 associated with the MICOS complex, SLC25A46 knockout did not change the abundance of MICOS components; this seemed to have little effect on cristae morphology (Abrams *et al.*, 2015; Wan *et al.*, 2016). Abrams and colleagues describe SLC25A46 as a Ugo1-like, OM carrier–like protein that interacts with the yeast MFN1/MFN2 counterpart, Fzo1, and with the MICOS complex component Fcj1 (Sesaki and Jensen, 2004; Harner *et al.*, 2011; Abrams *et al.*, 2015). However, deletion of Ugo1 results in mitochondrial fusion defects, reduced levels and oligomerization of Fzo1, and altered cristae morphology (Sesaki and Jensen, 2004; Harner *et al.*, 2011); this is the opposite of the SLC25A46 knockout phenotype that we describe here. Ugo1 is also suggested to regulate the local lipid composition in the OM, thereby facilitating mitochondrial fusion (Hoppins *et al.*, 2009). However, we did not detect differences in the mitochondrial phospholipid profile in cells lacking SLC25A46. Furthermore, Ugo1 seems to be important for linking Fzo1 with the IM MICOS subunit Fcj1 and regulating IM and OM fusion (Sesaki and Jensen, 2004; Harner *et al.*, 2011). A recent study suggests that SLC25A46 also functions with the MICOS complex, mediates lipid trafficking, and regulates mitochondrial respiration (Janer *et al.*, 2016). However, we did not report the same phenotype.

A potential reason for the different phenotypes might be the cell type studied, which emphasizes that mitochondrial dynamics pathways function differently in different cell types. Janer *et al.* (2016) primarily studied phenotypes in patient fibroblasts, in contrast to our studies in a variety of transformed cell types, including neuronal cells. We conclude that a subset of functions between SLC25A46 and Ugo1 may be conserved, whereas other functions developed differently; this is also likely a reflection of the increased complexity of multicellular organisms versus yeast. SLC25A46 interacts with a large number of proteins involved in mitochondrial ultrastructure, likely in transient complexes that were stabilized by cross-linking. Similar results were described for Ugo1 because Ugo1 interactions with Fzo1 and Mgm1 were also detected only after cross-linking (Wong *et al.*, 2003). Therefore SLC25A46 might function as a coordination point to facilitate rapid changes in mitochondrial ultrastructure in response to changes in the microenvironment by regulating the stability, assembly, and disassembly of proteins important for mitochondrial dynamics and cristae morphology.

Regulating the levels of SLC25A46 also seems to be important for its function. Our analysis shows that both MARCH5 and MULAN are ubiquitin ligases that contribute to the selective and rapid degradation of SLC25A46 L341P. Moreover, the ubiquitylated

SLC25A46 is subsequently removed from the mitochondrial OM via P97 and degraded by the proteasome, leading to an almost SLC25A46-null allele. The UPS has been described for the degradation of certain native OM proteins such as MFN1, MFN2, and MCL1 under stress conditions such as apoptosis or mitophagy (Ling and Jarvis, 2013). However, very little is understood about the selective degradation of OM proteins that fail to reach their native conformation. Thus our study expands the role of the UPS in a protein quality control pathway for the removal of misfolded proteins from the mitochondrial OM.

We speculate that point mutations such as L341P or P333L locate to important regions of SLC25A46, and mutant SLC25A46 signals to the UPS for rapid removal. This is akin to the pathway for removal of mutant plasma membrane protein cystic fibrosis transmembrane conductance regulator (CFTR). Specifically, the single amino acid deletion of phenylalanine 508 in CFTR results in retention in the ER and subsequent degradation by the UPS (Younger *et al.*, 2006; Morito *et al.*, 2008). Based on our results, organelles have developed similar quality control pathways using organelle-specific ubiquitin ligases and the cytosolic components of the UPS to deal with misfolded proteins. The mass spectrometry data (Supplemental Table S1) and coIP experiments (Figure 2A) indicated that the two E3 ubiquitin ligases MULAN and MARCH5 were primary candidates to initiate removal of SLC25A46 L341P. Cells with single knockdowns of MULAN or MARCH5 showed partial stabilization of SLC25A46 L341P, whereas decreasing active MULAN and MARCH5 together resulted in marked stabilization of SLC25A46 L341P with reduced ubiquitylation. Because the point mutation in SLC25A46 likely resides in the membrane environment, MULAN and MARCH5, both integral OM proteins, are the likely players for monitoring assembly of OM proteins (Campello *et al.*, 2014). MARCH5 and MULAN seem to have partially overlapping activities and coordinate ubiquitylation of SLC25A46.

SLC25A46's role in the regulation of assembly and disassembly of proteins in dynamics and cristae morphology seems to be very important for neuronal development. Mutations L341P and P333L caused fast turnover of SLC25A46 and result in severe malformation of the cerebellum and motor neurons and finally early death. In contrast, mutations at R340C, E335D, and G249D resulted in a protein with greater stability, and patients had milder phenotypes (Abrams *et al.*, 2015; Wan *et al.*, 2016). Specifically, those patients developed to adulthood and suffered from neuronal diseases such as CMT type 2A and DOA, which are also caused by mutations in mitochondrial dynamics proteins (Alexander *et al.*, 2000; Züchner *et al.*, 2004; Abrams *et al.*, 2015). Thus it is of great interest that SLC25A46 carrying those mutations was much more stable than SLC25A46 carrying mutation L341P or P333L (Wan *et al.*, 2016). Therefore the effect of mutations in SLC25A46 on neuronal development highly correlates with how the mutation destabilizes the protein. Again, this was verified with another family, in which a homozygous deletion of 1897 nucleotides within the SLC25A46 gene resulted in cerebellar malformation and early death as well (Wan *et al.*, 2016). The deletion resulted in loss of exon 1, which contained the start codon ATG for the longest and most prominent transcript and thus resulted in a gene knockout. These studies support an essential role of SLC25A46 in neuronal development. In sum, this analysis shows that the rapid degradation of SCL25A46 L341P likely causes pontocerebellar hypoplasia, a neuronal disease affecting mostly the cerebellum and motor neurons (Wan *et al.*, 2016), by disrupting the fine balance between fission and fusion in the mitochondrial network. This is in agreement with the observation that defects in fusion-mediating MFN2, which is regulated by SLC25A46, drastically disrupt the development and maturation of cerebellar Purkinje neurons (Chen *et al.*, 2007).

MATERIALS AND METHODS

Cell culture and transfection

HeLa (American Type Culture Collection [ATCC]), HEK293 T-REx Flp-In (Life Technologies), HEK293T (ATCC), LAN5 (provided by Joan Valentine, University of California, Los Angeles [UCLA], Los Angeles, CA), and HCT116 (provided by Richard Youle, National Institutes of Health, Bethesda, MD) were cultured in DMEM (high glucose, sodium pyruvate), RPMI (Life Technologies), and McCoy's 5A (GE Healthcare) media, respectively, and grown at 37°C in 5% CO_2. Media were supplemented with 10% fetal bovine serum (Atlanta Biological), 100 U/ml penicillin, and 100 µg/ml streptomycin (Life Technologies). Transfections were performed using BioT transfection reagent (Bioland) or Lipofectamine 2000 (Thermo Fisher Scientific) according to the manufacturer's instructions.

Chemicals and antibodies

MG132 (Enzo Biochem), NMS873 (Selleck Chemicals), bortezomib, bafilomycin A1, and MLN4924 (EMD Millipore) were dissolved in DMSO, stored at −80°C, and used at the indicated concentrations. DMSO at 0.1% served as the vehicle control.

Antibodies used in this study were SLC25A46 (Proteintech); HA (HA.11; Biolegend); MFN1 (ab57602) and histidine (HIS.H8; Abcam); LC3A/B (Cell Signaling); MFN2 (D1E9; Cell Signaling); MTCH2 (Abgent); MIC60/IMMT (Abgent and Proteintech); MID51 (Proteintech); Ubiquitin (FK2, Enzo Biochem); Mortalin (University of California, Davis/National Institutes of Health NeuroMab Facility); MIC19/CHCHD3 (Everest Biotech); MIC27/Apool (Assay BioTech); OPA1, P97/VCP, and TIMM23 (BD Biosciences); TOMM20 (FL-145), LRP130 (H-300), and glyceraldehyde-3-phosphate dehydrogenase (FL-335; Santa Cruz Biotechnology); MULAN (HPA017681) and Flag (M2) (Sigma-Aldrich); MARCH5 (provided by Richard Youle); myc (9E10; Developmental Studies Hybridoma Bank, University of Iowa); and Cullin 4a (PA5-29857; Thermo Fisher Scientific). PREP, GFP, TOMM40, YME1L, and PNPase polyclonal antibodies were raised against recombinant proteins (Pacific Immunology).

Genome editing by CRISPR/Cas9

We transfected 10^6 HCT116 or HEK293 T-REx Flp-In cells in a six-well plate with constructs coding for *SLC25A46*, *MUL1*, and *MARCH5* guide RNAs (gRNAs) and Cas9 endonuclease using BioT (Bioland) according to manufacturer's protocol. After 24 h, the cells were split into 6-cm dishes and selected with 2 µg/ml puromycin for 2 d. Puromycin was removed, and cells were grown in puromycin-free medium to confluency. Single-cell colonies were obtained by plating at 0.5 cell per 96 well. Colonies were expanded and analyzed by a T7 endonuclease cleavage assay, DNA sequencing, and immunoblotting.

Pulse-chase assays with cycloheximide

Cells were treated with 50 µg/ml cycloheximide (Sigma-Aldrich) for 0, 15, and 30 min. Where indicated, additional inhibitors were added at the same time as cycloheximide (MG132 or NMS873) or 1 h before the addition of cycloheximide (MLN4924). At each time point, cells were washed once with homogenization buffer (20 mM 4-(2-hydroxyethyl)-1-piperazineethanesulfonic acid, pH 7.4, 220 mM mannitol, 70 mM sucrose, 0.5 mM phenylmethylsulfonyl fluoride, 2.5 mM NaF, 1 mM Na_3VO_4, 10 mM *N*-ethylmaleimide, and 10 µM MG132), scraped in homogenization buffer using a Teflon cell lifter, transferred to 1.5-ml tube, and flash frozen in liquid nitrogen. Frozen pellets were stored at −80°C until mitochondria were isolated.

Biochemical assays

Standard protocols were used for mass spectrometry and biochemical experiments with mitochondria. For detailed protocols, see the Supplemental Materials and Methods.

ACKNOWLEDGMENTS

We thank Elke Krüger (Charité, Berlin), Richard Youle (National Institutes of Health, Bethesda, MD), Mariusz Karbowski (University of Maryland, College Park, MD), Alexander van der Bliek (UCLA, Los Angeles, CA), Joan Valentine (UCLA), and Ming Guo (UCLA) for valuable reagents. Technical assistance was provided by Luke Batty. This research was supported by National Institutes of Health Grant GM61721 and California Stem Cell Agency Grant RT307678 to C.M.K., National Institutes of Health Grants HL108882 and GM111548 to S.M.C. and GM089778 to J.A.W., National Institutes of Health Grant R01 NS064183, National Center for Advancing Translational Sciences UCLA CTSI Grant UL1TR000124, and UCLA Children's Discovery and Innovation Institute Award to J.C.J., and Deutsche Forschungsgemeinschaft Grant STE 2045/1-1 to J.S.

REFERENCES

Abrams AJ, Hufnagel RB, Rebelo A, Zanna C, Patel N, Gonzalez MA, Campeanu IJ, Griffin LB, Groenewald S, Strickland AV, *et al.* (2015). Mutations in SLC25A46, encoding a UGO1-like protein, cause an optic atrophy spectrum disorder. Nat Genet 47, 926–932.

Alexander C, Votruba M, Pesch UE, Thiselton DL, Mayer S, Moore A, Rodriguez M, Kellner U, Leo-Kottler B, Auburger G, *et al.* (2000). OPA1, encoding a dynamin-related GTPase, is mutated in autosomal dominant optic atrophy linked to chromosome 3q28. Nat Genet 26, 211–215.

Ambivero CT, Cilenti L, Main S, Zervos AS (2014). Mulan E3 ubiquitin ligase interacts with multiple E2 conjugating enzymes and participates in mitophagy by recruiting GABARAP. Cell Signal 26, 2921–2929.

Anton F, Fres JM, Schauss A, Pinson B, Praefcke GJ, Langer T, Escobar-Henriques M (2011). Ugo1 and Mdm30 act sequentially during Fzo1-mediated mitochondrial outer membrane fusion. J Cell Sci 124, 1126–1135.

Archer SL (2013). Mitochondrial dynamics-mitochondrial fission and fusion in human diseases. N Engl J Med 369, 2236–2251.

Bae S, Kim SY, Jung JH, Yoon Y, Cha HJ, Lee H, Kim K, Kim J, An IS, Um HD, *et al.* (2012). Akt is negatively regulated by the MULAN E3 ligase. Cell Res 22, 873–885.

Bertholet AM, Delerue T, Millet AM, Moulis MF, David C, Daloyau M, Arnaune-Pelloquin L, Davezac N, Mils V, Miquel MC, *et al.* (2016). Mitochondrial fusion/fission dynamics in neurodegeneration and neuronal plasticity. Neurobiol Dis 90, 3–19.

Bohnert M, Zerbes RM, Davies KM, Muhleip AW, Rampelt H, Horvath SE, Boenke T, Kram A, Perschil I, Veenhuis M, *et al.* (2015). Central role of Mic10 in the mitochondrial contact site and cristae organizing system. Cell Metab 21, 747–755.

Braschi E, Zunino R, McBride HM (2009). MAPL is a new mitochondrial SUMO E3 ligase that regulates mitochondrial fission. EMBO Rep 10, 748–754.

Brownell JE, Sintchak MD, Gavin JM, Liao H, Bruzzese FJ, Bump NJ, Soucy TA, Milhollen MA, Yang X, Burkhardt AL, *et al.* (2010). Substrate-assisted inhibition of ubiquitin-like protein-activating enzymes: the NEDD8 E1 inhibitor MLN4924 forms a NEDD8-AMP mimetic in situ. Mol Cell 37, 102–111.

Campello S, Strappazzon F, Cecconi F (2014). Mitochondrial dismissal in mammals, from protein degradation to mitophagy. Biochim Biophys Acta 1837, 451–460.

Chen H, Detmer SA, Ewald AJ, Griffin EE, Fraser SE, Chan DC (2003). Mitofusins Mfn1 and Mfn2 coordinately regulate mitochondrial fusion and are essential for embryonic development. J Cell Biol 160, 189–200.

Chen H, McCaffery JM, Chan DC (2007). Mitochondrial fusion protects against neurodegeneration in the cerebellum. Cell 130, 548–562.

Delettre C, Griffoin JM, Kaplan J, Dollfus H, Lorenz B, Faivre L, Lenaers G, Belenguer P, Hamel CP (2001). Mutation spectrum and splicing variants in the OPA1 gene. Hum Genet 109, 584–591.

Detmer SA, Chan DC (2007). Complementation between mouse Mfn1 and Mfn2 protects mitochondrial fusion defects caused by CMT2A disease mutations. J Cell Biol 176, 405–414.

DeVay RM, Dominguez-Ramirez L, Lackner LL, Hoppins S, Stahlberg H, Nunnari J (2009). Coassembly of Mgm1 isoforms requires cardiolipin and mediates mitochondrial inner membrane fusion. J Cell Biol 186, 793–803.

Emanuele MJ, Elia AE, Xu Q, Thoma CR, Izhar L, Leng Y, Guo A, Chen YN, Rush J, Hsu PW, *et al.* (2011). Global identification of modular cullin-RING ligase substrates. Cell 147, 459–474.

Friedman JR, Mourier A, Yamada J, McCaffery JM, Nunnari J (2015). MICOS coordinates with respiratory complexes and lipids to establish mitochondrial inner membrane architecture. Elife 4, 10.7554/eLife.07739.

Haitina T, Lindblom J, Renstrom T, Fredriksson R (2006). Fourteen novel human members of mitochondrial solute carrier family 25 (SLC25) widely expressed in the central nervous system. Genomics 88, 779–790.

Harner M, Korner C, Walther D, Mokranjac D, Kaesmacher J, Welsch U, Griffith J, Mann M, Reggiori F, Neupert W (2011). The mitochondrial contact site complex, a determinant of mitochondrial architecture. EMBO J 30, 4356–4370.

Heo JM, Livnat-Levanon N, Taylor EB, Jones KT, Dephoure N, Ring J, Xie J, Brodsky JL, Madeo F, Gygi SP, *et al.* (2010). A stress-responsive system for mitochondrial protein degradation. Mol Cell 40, 465–480.

Hoppins S, Horner J, Song C, McCaffery JM, Nunnari J (2009). Mitochondrial outer and inner membrane fusion requires a modified carrier protein. J Cell Biol 184, 569–581.

Hwang DK, Claypool SM, Leuenberger D, Tienson HL, Koehler CM (2007). Tim54p connects inner membrane assembly and proteolytic pathways in the mitochondrion. J Cell Biol 178, 1161–1175.

Ishihara N, Fujita Y, Oka T, Mihara K (2006). Regulation of mitochondrial morphology through proteolytic cleavage of OPA1. EMBO J 25, 2966–2977.

Janer A, Prudent J, Paupe V, Fahiminiya S, Majewski J, Sgarioto N, Des Rosiers C, Forest A, Lin ZY, Gingras AC, *et al.* (2016). SLC25A46 is required for mitochondrial lipid homeostasis and cristae maintenance and is responsible for Leigh syndrome. EMBO Mol Med 8, 1019–1038.

Karbowski M, Neutzner A, Youle RJ (2007). The mitochondrial E3 ubiquitin ligase MARCH5 is required for Drp1 dependent mitochondrial division. J Cell Biol 178, 71–84.

Karbowski M, Youle RJ (2011). Regulating mitochondrial outer membrane proteins by ubiquitination and proteasomal degradation. Curr Opin Cell Biol 23, 476–482.

Kisselev AF, Goldberg AL (2001). Proteasome inhibitors: from research tools to drug candidates. Chem Biol 8, 739–758.

Leboucher GP, Tsai YC, Yang M, Shaw KC, Zhou M, Veenstra TD, Glickman MH, Weissman AM (2012). Stress-induced phosphorylation and proteasomal degradation of mitofusin 2 facilitates mitochondrial fragmentation and apoptosis. Mol Cell 47, 547–557.

Ling Q, Jarvis P (2013). Dynamic regulation of endosymbiotic organelles by ubiquitination. Trends Cell Biol 23, 399–408.

Livnat-Levanon N, Glickman MH (2011). Ubiquitin-proteasome system and mitochondria - reciprocity. Biochim Biophys Acta 1809, 80–87.

Lokireddy S, Wijesoma IW, Teng S, Bonala S, Gluckman PD, McFarlane C, Sharma M, Kambadur R (2012). The ubiquitin ligase Mul1 induces mitophagy in skeletal muscle in response to muscle-wasting stimuli. Cell Metab 16, 613–624.

Magnaghi P, D'Alessio R, Valsasina B, Avanzi N, Rizzi S, Asa D, Gasparri F, Cozzi L, Cucchi U, Orrenius C, *et al.* (2013). Covalent and allosteric inhibitors of the ATPase VCP/p97 induce cancer cell death. Nat Chem Biol 9, 548–556.

Moore BS, Eustaquio AS, McGlinchey RP (2008). Advances in and applications of proteasome inhibitors. Curr Opin Chem Biol 12, 434–440.

Morito D, Hirao K, Oda Y, Hosokawa N, Tokunaga F, Cyr DM, Tanaka K, Iwai K, Nagata K (2008). Gp78 cooperates with RMA1 in endoplasmic reticulum-associated degradation of CFTRDeltaF508. Mol Biol Cell 19, 1328–1336.

Nakamura N, Kimura Y, Tokuda M, Honda S, Hirose S (2006). MARCH-V is a novel mitofusin 2- and Drp1-binding protein able to change mitochondrial morphology. EMBO Rep 7, 1019–1022.

Narendra D, Tanaka A, Suen DF, Youle RJ (2008). Parkin is recruited selectively to impaired mitochondria and promotes their autophagy. J Cell Biol 183, 795–803.

Okuda-Shimizu Y, Hendershot LM (2007). Characterization of an ERAD pathway for nonglycosylated BiP substrates, which require Herp. Mol Cell 28, 544–554.

Quiros PM, Langer T, Lopez-Otin C (2015). New roles for mitochondrial proteases in health, ageing and disease. Nat Rev Mol Cell Biol 16, 345–359.
Santel A, Fuller MT (2001). Control of mitochondrial morphology by a human mitofusin. J Cell Sci 114, 867–874.
Sesaki H, Jensen RE (2004). Ugo1p links the Fzo1p and Mgm1p GTPases for mitochondrial fusion. J Biol Chem 279, 28298–28303.
Soucy TA, Smith PG, Milhollen MA, Berger AJ, Gavin JM, Adhikari S, Brownell JE, Burke KE, Cardin DP, Critchley S, *et al.* (2009). An inhibitor of NEDD8-activating enzyme as a new approach to treat cancer. Nature 458, 732–736.
Tanaka A, Cleland MM, Xu S, Narendra DP, Suen DF, Karbowski M, Youle RJ (2010). Proteasome and p97 mediate mitophagy and degradation of mitofusins induced by Parkin. J Cell Biol 191, 1367–1380.
Tsubuki S, Saito Y, Tomioka M, Ito H, Kawashima S (1996). Differential inhibition of calpain and proteasome activities by peptidyl aldehydes of di-leucine and tri-leucine. J Biochem 119, 572–576.
Verhoeven K, Claeys KG, Zuchner S, Schroder JM, Weis J, Ceuterick C, Jordanova A, Nelis E, De Vriendt E, Van Hul M, *et al.* (2006). MFN2 mutation distribution and genotype/phenotype correlation in Charcot-Marie-Tooth type 2. Brain 129, 2093–2102.
Wan J, Steffen J, Yourshaw M, Mamsa H, Andersen E, Rudnik-Schöneborn S, Pope K, Howell KB, McLean CA, Kornberg AJ, *et al.* (2016). Loss of function of SLC25A46 causes lethal congenital pontocerebellar hypoplasia. Brain 139, 2877–2890.
Wong ED, Wagner JA, Scott SV, Okreglak V, Holewinske TJ, Cassidy-Stone A, Nunnari J (2003). The intramitochondrial dynamin-related GTPase, Mgm1p, is a component of a protein complex that mediates mitochondrial fusion. J Cell Biol 160, 303–311.
Yonashiro R, Ishido S, Kyo S, Fukuda T, Goto E, Matsuki Y, Ohmura-Hoshino M, Sada K, Hotta H, Yamamura H, *et al.* (2006). A novel mitochondrial ubiquitin ligase plays a critical role in mitochondrial dynamics. EMBO J 25, 3618–3626.
Younger JM, Chen L, Ren HY, Rosser MF, Turnbull EL, Fan CY, Patterson C, Cyr DM (2006). Sequential quality-control checkpoints triage misfolded cystic fibrosis transmembrane conductance regulator. Cell 126, 571–582.
Yun J, Puri R, Yang H, Lizzio MA, Wu C, Sheng ZH, Guo M (2014). MUL1 acts in parallel to the PINK1/parkin pathway in regulating mitofusin and compensates for loss of PINK1/parkin. Elife 3, e01958.
Zhang B, Huang J, Li HL, Liu T, Wang YY, Waterman P, Mao AP, Xu LG, Zhai Z, Liu D, *et al.* (2008). GIDE is a mitochondrial E3 ubiquitin ligase that induces apoptosis and slows growth. Cell Res 18, 900–910.
Züchner S, Mersiyanova IV, Muglia M, Bissar-Tadmouri N, Rochelle J, Dadali EL, Zappia M, Nelis E, Patitucci A, Senderek J, *et al.* (2004). Mutations in the mitochondrial GTPase mitofusin 2 cause Charcot-Marie-Tooth neuropathy type 2A. Nat Genet 36, 449–451.